Coordinated Adaptive Robust Contouring Control of an Industrial Biaxial Precision Gantry With Cogging Force Compensations

Chuxiong Hu, *Student Member, IEEE*, Bin Yao, *Senior Member, IEEE*, and Qingfeng Wang

***Abstract*—Cogging force is an important source of disturbances for linear-motor-driven systems. To obtain a higher level of contouring motion control performance for multiaxis mechanical systems subject to significant nonlinear cogging forces, both the coordinated control of multiaxis motions and the effective compensation of cogging forces are necessary. In addition, the effect of unavoidable velocity measurement noises needs to be sufficiently attenuated. This paper presents a discontinuous-projection-based desired compensation adaptive robust contouring controller to address these control issues all at once. Specifically, the presented approach explicitly takes into account the specific characteristics of cogging forces in the controller designs and employs the task coordinate formulation for coordinated motion controls. Theoretically, the resulting controller achieves a guaranteed transient performance and a steady-state contouring accuracy even in the presence of both parametric uncertainties and uncertain nonlinearities. In addition, the controller also achieves asymptotic output tracking when there are parametric uncertainties only. Comparative experimental results obtained on a high-speed Anorad industrial biaxial precision gantry are presented to verify the excellent contouring performance of the proposed control scheme and the effectiveness of the cogging force compensations.**

***Index Terms*—Adaptive control, cogging force, contouring control, linear motor.**

I. Introduction

CONTOURING performance is evaluated by the contouring error which represents the geometric deviation from the actual contour to the desired contour [1]. The degradation of contouring performance [2] could be mainly due to either the lack of coordination among multiaxis motions [3] or the effects of disturbances such as friction [4]–[6] and ripple forces [7], [8]. The former is referred to as the coordinated contouring control problem and the latter as the disturbance rejection/compensation.

Manuscript received March 24, 2009; revised August 13, 2009. First published August 28, 2009; current version published April 14, 2010. This work was supported in part by the U.S. National Science Foundation under Grant CMS-0600516, in part by the National Natural Science Foundation of China under the Joint Research Fund for Overseas Chinese Young Scholars under Grant 50528505, and in part by the Ministry of Education of China through a Chang Jiang Chair Professorship.

C. Hu and Q. Wang are with the State Key Laboratory of Fluid Power Transmission and Control, Zhejiang University, Hangzhou 310027, China (e-mail: fyfox.hu@gmail.com; qfwang@zju.edu.cn).

B. Yao is with the School of Mechanical Engineering, Purdue University, West Lafayette, IN 47907 USA, and also with the State Key Laboratory of Fluid Power Transmission and Control, Zhejiang University, Hangzhou 310027, China (e-mail: byao@purdue.edu).

Color versions of one or more of the figures in this paper are available online at http://ieeexplore.ieee.org.

Digital Object Identifier 10.1109/TIE.2009.2030769

Both the contouring control problem and the disturbance rejection/compensation problem have been extensively studied individually. Specifically, as opposed to the traditional decoupled control such as [9] and [10], earlier research works on the coordinated contouring control [11]–[14] use the cross-coupled control strategy [15]. Later on, the contouring control problem is formulated in a task coordinate frame by using either of the following: 1) the concept of generalized curvilinear coordinates introduced in [16], which is done in [17] and [18], or 2) the *locally* defined coordinates "attached" to the desired contour proposed in [3]. Under the task coordinate formulation, a control law could be designed to assign different dynamics to the normal and tangential directions relative to the desired contour. Since then, many contouring control schemes based on task coordinate approaches have been reported [1], [19]. However, all these latest publications on coordinated control techniques cannot explicitly deal with parametric uncertainties and uncertain nonlinearities. As a result, they are often insufficient when stringent contouring performance is of concern, as actual systems are always subjected to certain model uncertainties and disturbances.

In controlling linear-motor-driven systems, cogging force is known as an important source of disturbances. To achieve higher precision of motion, the cogging force behavior should be clearly understood such that effective cogging force compensation can be synthesized. Thus, significant research efforts have been devoted to the modeling and compensation of cogging forces as well. For example, in [20]–[22], the cogging force is assumed to be periodic functions with respect to position so that Fourier expansion with a few significant terms could be utilized to represent the cogging force. A nonperiodic effect is also considered in a recent publication [23]. It should be noted that all these cogging force compensation research works are done for single axis motion only.

During the past decade, an adaptive robust control (ARC) framework has been developed by Yao and Tomizuka in [24]–[26] to provide a rigorous theoretic framework for the precision motion control of systems with both parametric uncertainties and uncertain nonlinearities. The approach effectively integrates the traditional robust adaptive controls and the deterministic robust controls, and achieves a guaranteed transient and steady-state output tracking performance without losing the asymptotic output tracking capability of adaptive designs. The desired compensation ARC (DCARC) strategy has also been proposed in [27] and [28] to reduce the effect of measurement noises.

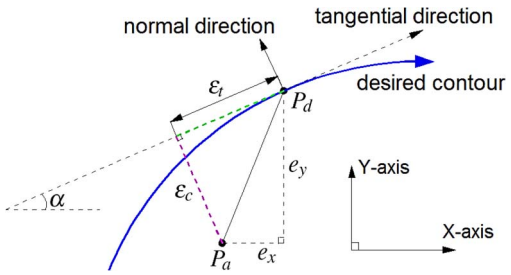

Fig. 1. Approximate contouring error model.

In [29], the ARC strategy [24] and the task coordinate frame approach in [3] have been integrated to develop a high-performance contouring controller for high-speed machines. To obtain a higher level of contouring motion control performance for linear-motor-driven multiaxis mechanical systems subject to significant nonlinear cogging forces, both the coordinated control of multiaxis motions and the effective compensation of cogging forces are necessary. In addition, the effect of unavoidable velocity measurement noises needs to be carefully examined and sufficiently attenuated. This paper presents a holistic approach to address all these issues at once. Specifically, a discontinuous-projection-based desired compensation adaptive robust contouring controller is presented. The proposed approach explicitly takes into account the specific characteristics of cogging forces in the controller designs and employs the task coordinate formulation for coordinated motion controls. Experimental results have also been obtained on a high-speed Anorad industrial biaxial gantry driven by LC-50-200 linear motors with a linear encoder resolution of 0.5 μm. The results verify the excellent contouring performance of the proposed DCARC controller in an actual implementation in spite of various parametric uncertainties and uncertain disturbances. Comparative experimental results also demonstrate the effectiveness of the cogging force compensations.

II. Problem Formulation

A. Task Coordinate Frame

Since an accurate calculation of contouring error often leads to an intensive computation task which is hard to be realized in practice, various approximations have been used in the contouring controls instead. Fig. 1 shows a popular approximation of contouring error [12], [19]. Let x and y denote the horizontal and vertical axes of a biaxial gantry system. At any time instant, there are two points P_d and P_a denoting the position of the reference command and the actual position of the system, respectively. Tangential and normal directions of the desired contour at point P_d are used to approximate the contouring error by the distance from P_a to the tangential line. With this definition, the contouring error ε_c can be approximately computed by the normal error ε_n as

$$\varepsilon_c \approx \varepsilon_n = -\sin\alpha \cdot e_x + \cos\alpha \cdot e_y \tag{1}$$

where e_x and e_y denote the axial tracking errors of x- and y-axes, i.e., $e_x = x - x_d$ and $e_y = y - y_d$, and α denotes the angle between the tangential line to the horizontal X-axis. This way of approximating the contouring error is reasonable when the axial tracking errors are comparatively small to the curvature of the desired contour.

The tangential error ε_t in Fig. 1 can be obtained as

$$\varepsilon_t = \cos\alpha \cdot e_x + \sin\alpha \cdot e_y. \tag{2}$$

As the tangential and normal directions are mutually orthogonal, they can be taken as the basis for the task coordinate frame. Thus, the physical (x, y) coordinates can be transformed into the task coordinates of $(\varepsilon_c, \varepsilon_t)$ by a linear transformation

$$\varepsilon = \mathbf{T}\mathbf{e}, \qquad \mathbf{T} = \begin{bmatrix} -\sin\alpha & \cos\alpha \\ \cos\alpha & \sin\alpha \end{bmatrix} \tag{3}$$

where $\varepsilon = [\varepsilon_c, \varepsilon_t]^{\mathrm{T}}$, and $\mathbf{e} = [e_x, e_y]^{\mathrm{T}}$. Note that the time-varying transformation matrix $\mathbf{T}$ depends on the reference trajectories of the desired contour only and is unitary for all values of α, i.e., $\mathbf{T^T} = \mathbf{T}$ and $\mathbf{T^{-1}} = \mathbf{T}$.

B. System Dynamics

The dynamics of the biaxial linear-motor-driven gantry can be described by [30]

$$\mathbf{M}\ddot{\mathbf{q}} + \mathbf{B}\dot{\mathbf{q}} + \mathbf{F_c}(\dot{\mathbf{q}}) + \mathbf{F_r}(\mathbf{q}) = \mathbf{u} + \mathbf{d} \tag{4}$$

where $\mathbf{q} = [x(t), y(t)]^{\mathrm{T}}$, $\dot{\mathbf{q}} = [\dot{x}(t), \dot{y}(t)]^{\mathrm{T}}$, and $\ddot{\mathbf{q}} = [\ddot{x}(t), \ddot{y}(t)]^{\mathrm{T}}$ are the 2×1 vectors of the axis position, velocity, and acceleration, respectively; $\mathbf{M} = \mathrm{diag}[M_1, M_2]$ and $\mathbf{B} = \mathrm{diag}[B_1, B_2]$ are the 2×2 diagonal inertia and viscous friction coefficient matrices, respectively. $\mathbf{F_c}(\dot{\mathbf{q}})$ is the 2×1 vector of Coulomb friction, which is modeled by $\mathbf{F_c}(\dot{\mathbf{q}}) = \mathbf{A_f}\mathbf{S_f}(\dot{\mathbf{q}})$, where $\mathbf{A_f} = \mathrm{diag}[A_{f1}, A_{f2}]$ is the 2×2 unknown diagonal Coulomb friction coefficient matrix and $\mathbf{S_f}(\dot{\mathbf{q}})$ is a known vector-valued smooth function used to approximate the traditional discontinuous sign function $\mathrm{sgn}(\dot{\mathbf{q}})$ used in the traditional Coulomb friction modeling for effective friction compensation in implementation [20]. $\mathbf{F_r}(\mathbf{q})$ represents the 2×1 vector of position dependent cogging forces. $\mathbf{u}$ is the 2×1 vector of control input, and $\mathbf{d}$ is the 2×1 vector of unknown nonlinear functions due to external disturbances or modeling errors.

In this paper, it is assumed that the permanent magnets of a linear motor are all identical and equally spaced at a pitch of P. Thus, $\mathbf{F_r}(\mathbf{q}) = [F_{rx}(x), F_{ry}(y)]^{\mathrm{T}}$ is a periodic function of position $\mathbf{q}$ with a period of P, i.e., $F_{rx}(x + P) = F_{rx}(x)$, $F_{ry}(y + P) = F_{ry}(y)$, and it can be approximated quite accurately by the first several harmonic functions of the positions given by [20]

$$\begin{aligned} \overline{F}_{rx}(x) &= \sum_{i=1}^{m} \left(S_{xi} \sin\left(\frac{2i\pi}{P}x\right) + C_{xi} \cos\left(\frac{2i\pi}{P}x\right) \right) \\ \overline{F}_{ry}(y) &= \sum_{j=1}^{n} \left(S_{yj} \sin\left(\frac{2j\pi}{P}y\right) + C_{yj} \cos\left(\frac{2j\pi}{P}y\right) \right) \end{aligned} \tag{5}$$

where S_{xi}, C_{xi}, S_{yj}, and C_{yj} are the unknown weights, and m and n are the numbers of harmonics used to approximate

the cogging forces in X- and Y-axes, respectively. With these cogging force and friction models, the linear motor dynamics (4) can be rewritten as

$$\mathbf{M}\ddot{\mathbf{q}} + \mathbf{B}\dot{\mathbf{q}} + \mathbf{A_f}\mathbf{S_f}(\dot{\mathbf{q}}) + \overline{\mathbf{F}}_\mathbf{r}(\mathbf{q}) = \mathbf{u} + \mathbf{d_N} + \widetilde{\mathbf{d}} \quad (6)$$

where $\mathbf{d_N} = [d_{N1}, d_{N2}]^{\mathrm{T}}$ is the nominal value of the lumped modeling error and disturbance $\mathbf{d}_l = \mathbf{d} + \overline{\mathbf{F}}_\mathbf{r}(\mathbf{q}) - \mathbf{F_r}(\mathbf{q}) + \mathbf{A_f}\mathbf{S_f}(\dot{\mathbf{q}}) - \mathbf{F_c}(\dot{\mathbf{q}})$, and $\widetilde{\mathbf{d}} = \mathbf{d}_l - \mathbf{d}_N$ represents the time-varying portion of the lumped uncertainties. Define the axis tracking error vector as $\mathbf{e} = [e_x, e_y]^{\mathrm{T}} = [x(t) - x_d(t), y(t) - y_d(t)]^{\mathrm{T}}$, where $\mathbf{q_d}(t) = [x_d(t), y_d(t)]^{\mathrm{T}}$ is the reference trajectory describing the desired contour. Then, the system dynamics can be written in terms of $\mathbf{e}$ as

$$\mathbf{M}\ddot{\mathbf{e}} + \mathbf{B}\dot{\mathbf{e}} + \mathbf{A_f}\mathbf{S_f}(\dot{\mathbf{q}}) + \overline{\mathbf{F}}_\mathbf{r}(\mathbf{q}) + \mathbf{M}\ddot{\mathbf{q}}_\mathbf{d} + \mathbf{B}\dot{\mathbf{q}}_\mathbf{d} = \mathbf{u} + \mathbf{d_N} + \widetilde{\mathbf{d}}. \quad (7)$$

Noting (3) and the unitary property of $\mathbf{T}$, the axis tracking errors are related to the task coordinates as [19]

$$\dot{\mathbf{e}} = \mathbf{T}\dot{\varepsilon} + \dot{\mathbf{T}}\varepsilon \qquad \ddot{\mathbf{e}} = \mathbf{T}\ddot{\varepsilon} + \mathbf{2}\dot{\mathbf{T}}\dot{\varepsilon} + \ddot{\mathbf{T}}\varepsilon. \quad (8)$$

The system dynamics can thus be represented in the task coordinate frame as

$$\mathbf{M_t}\ddot{\varepsilon} + \mathbf{B_t}\dot{\varepsilon} + 2\mathbf{C_t}\dot{\varepsilon} + \mathbf{D_t}\varepsilon + \mathbf{M_q}\ddot{\mathbf{q}}_\mathbf{d} + \mathbf{B_q}\dot{\mathbf{q}}_\mathbf{d} + \mathbf{A_{fq}}\mathbf{S_f}(\dot{\mathbf{q}}) + \mathbf{F_{rq}}(\mathbf{q}) = \mathbf{u_t} + \mathbf{d_t} + \widetilde{\Delta} \quad (9)$$

where

$$\begin{aligned} \mathbf{M_t} &= \mathbf{TMT} & \mathbf{B_t} &= \mathbf{TBT} & \mathbf{C_t} &= \mathbf{TM}\dot{\mathbf{T}} \\ \mathbf{D_t} &= \mathbf{TM}\ddot{\mathbf{T}} + \mathbf{TB}\dot{\mathbf{T}} & \mathbf{u_t} &= \mathbf{Tu} & \mathbf{d_t} &= \mathbf{Td_N} \\ \widetilde{\Delta} &= \mathbf{T}\widetilde{\mathbf{d}} & \mathbf{M_q} &= \mathbf{TM} & \mathbf{B_q} &= \mathbf{TB} \\ \mathbf{A_{fq}} &= \mathbf{TA_f} & \mathbf{F_{rq}}(\mathbf{q}) &= \mathbf{T}\overline{\mathbf{F}}_\mathbf{r}(\mathbf{q}). \end{aligned} \quad (10)$$

It is well known that (9) has the following properties [16].

(P1) $\mathbf{M_t}$ is a symmetric positive definite matrix with $\mu_1\mathbf{I} \leq \mathbf{M_t} \leq \mu_2\mathbf{I}$, where μ_1 and μ_2 are some positive scalars.

(P2) The matrix $\mathbf{N}_t = \mathbf{M_t} - \mathbf{2C_t}$ is a skew-symmetric matrix.

(P3) The matrices or vectors in (9), namely, $\mathbf{M_t}$, $\mathbf{B_t}$, $\mathbf{C_t}$, $\mathbf{D_t}$, $\mathbf{M_q}$, $\mathbf{B_q}$, $\mathbf{A_{fq}}$, $\mathbf{F_{rq}}(\mathbf{q})$, and $\mathbf{d_t}$, can be linearly parametrized by a set of parameters defined by $\theta = [\theta_1, \ldots, \theta_{8+2m+2n}]^{\mathrm{T}} = [M_1, M_2, B_1, B_2, A_{f1}, A_{f2}, S_{x1}, C_{x1}, \ldots, S_{xm}, C_{xm}, S_{y1}, C_{y1}, \ldots, S_{yn}, C_{yn}, d_{N1}, d_{N2}]^{\mathrm{T}}$.

In general, the parameter vector θ cannot be known exactly in advance due to factors such as the change of payloads of the biaxial gantry. However, the extent of parametric uncertainties can be predicted. Therefore, the following practical assumption is made.

Assumption 1: The extent of the parametric uncertainties and uncertain nonlinearities is known, i.e.,

$$\theta \in \Omega_\theta \triangleq \{\theta :\ \theta_{\min} \leq \theta \leq \theta_{\max}\} \quad (11)$$

$$\widetilde{\Delta} \in \Omega_\Delta \triangleq \left\{\widetilde{\Delta} :\ \|\widetilde{\Delta}\| \leq \delta_\Delta\right\} \quad (12)$$

where $\theta_{\min} = [\theta_{1\min}, \ldots, \theta_{(8+2m+2n)\min}]^{\mathrm{T}}$ and $\theta_{\max} = [\theta_{1\max}, \ldots, \theta_{(8+2m+2n)\max}]^{\mathrm{T}}$ are known constant vectors, and $\boldsymbol{\delta}_\Delta$ is a known function.

III. Discontinuous Projection

Let $\widehat{\theta}$ denote the estimate of θ and $\widetilde{\theta}$ the estimation error (i.e., $\widetilde{\theta} = \widehat{\theta} - \theta$). In view of (11), the following adaptation law with discontinuous projection modification can be used:

$$\dot{\widehat{\theta}} = Proj_{\widehat{\theta}}(\Gamma\tau) \quad (13)$$

where $\Gamma > 0$ is a diagonal matrix, and τ is an adaptation function to be synthesized later. The projection mapping $Proj_{\widehat{\theta}}(\bullet) = [Proj_{\widehat{\theta}_1}(\bullet_1), \ldots, Proj_{\widehat{\theta}_p}(\bullet_p)]^{\mathrm{T}}$ is defined in [24] as

$$Proj_{\widehat{\theta}_i}(\bullet_i) = \begin{cases} 0, & \text{if } \widehat{\theta}_i = \theta_{i\max} \text{ and } \bullet_i > 0 \\ 0, & \text{if } \widehat{\theta}_i = \theta_{i\min} \text{ and } \bullet_i < 0 \\ \bullet_i, & \text{if otherwise.} \end{cases} \quad (14)$$

It is shown that, for any adaptation function τ, the projection mapping used in (14) guarantees [25]

$$\text{(P4)} \qquad \widehat{\theta} \in \Omega_\theta \triangleq \{\widehat{\theta} : \theta_{i\min} \leq \widehat{\theta} \leq \theta_{i\max}\}$$

$$\text{(P5)} \qquad \widetilde{\theta}^{\mathrm{T}}\left(\Gamma^{-1}Proj_{\widehat{\theta}}(\Gamma\tau) - \tau\right) \leq 0 \qquad \forall\, \tau. \quad (15)$$

IV. ARC Law Synthesis

Define a switching-function-like quantity as

$$\mathbf{s} = \dot{\varepsilon} + \Lambda\varepsilon \quad (16)$$

where $\Lambda > 0$ is a diagonal matrix. Define a positive semidefinite (p.s.d.) function

$$V(t) = \frac{\mathbf{1}}{\mathbf{2}}\mathbf{s}^{\mathbf{T}}\mathbf{M_t}\mathbf{s}. \quad (17)$$

Differentiating V yields

$$\dot{V} = \mathbf{s}^{\mathbf{T}}\Big[\mathbf{u_t} + \mathbf{d_t} + \widetilde{\Delta} - \mathbf{M_q}\ddot{\mathbf{q}}_\mathbf{d} - \mathbf{B_q}\dot{\mathbf{q}}_\mathbf{d} - \mathbf{A_{fq}}\mathbf{S_f}(\dot{\mathbf{q}}) - \mathbf{F_{rq}}(\mathbf{q}) - \mathbf{B_t}\dot{\varepsilon} - \mathbf{C_t}\dot{\varepsilon} - \mathbf{D_t}\varepsilon + \mathbf{C_t}\boldsymbol{\Lambda}\varepsilon + \mathbf{M_t}\boldsymbol{\Lambda}\dot{\varepsilon}\Big] \quad (18)$$

where (P2) is used to eliminate the term $(\mathbf{1/2})\mathbf{s}^{\mathbf{T}}\dot{\mathbf{M}}_\mathbf{t}\mathbf{s}$. Furthermore, viewing (P3), we can linearly parameterize the terms in (18) as

$$\mathbf{M_q}\ddot{\mathbf{q}}_\mathbf{d} + \mathbf{B_q}\dot{\mathbf{q}}_\mathbf{d} + \mathbf{A_{fq}}\mathbf{S_f}(\dot{\mathbf{q}}) + \mathbf{F_{rq}}(\mathbf{q}) + \mathbf{B_t}\dot{\varepsilon} + \mathbf{C_t}\dot{\varepsilon} + \mathbf{D_t}\varepsilon - \mathbf{C_t}\Lambda\varepsilon - \mathbf{M_t}\Lambda\dot{\varepsilon} - \mathbf{d_t} = -\Psi(\mathbf{q}, \dot{\mathbf{q}}, t)\theta \quad (19)$$

where Ψ is a $2 \times (8 + 2m + 2n)$ matrix of known functions, known as the regressor. Thus, (18) can be rewritten as

$$\dot{V} = \mathbf{s}^{\mathbf{T}}\left[\mathbf{u_t} + \Psi(\mathbf{q}, \dot{\mathbf{q}}, t)\theta + \widetilde{\Delta}\right]. \quad (20)$$

Noting the structure of (20), the following ARC law is proposed:

$$\mathbf{u_t} = \mathbf{u_a} + \mathbf{u_s}, \quad \mathbf{u_a} = -\Psi(\mathbf{q}, \dot{\mathbf{q}}, t)\widehat{\theta} \quad (21)$$

where $\mathbf{u_a}$ is the adjustable model compensation needed for achieving perfect tracking, and $\mathbf{u_s}$ is a robust control law to be synthesized later. Substituting (21) into (20) and simplifying the resulting expression lead to

$$\dot{V} = \mathbf{s^T}\left[\mathbf{u_s} - \Psi(\mathbf{q}, \dot{\mathbf{q}}, t)\widetilde{\theta} + \widetilde{\Delta}\right]. \tag{22}$$

The robust control function $\mathbf{u_s}$ consists of two terms

$$\mathbf{u_s} = \mathbf{u_{s1}} + \mathbf{u_{s2}}, \quad \mathbf{u_{s1}} = -\mathbf{K}\mathbf{s} \tag{23}$$

where $\mathbf{u_{s1}}$ is used to stabilize the nominal system, which is chosen to be a simple proportional feedback with $\mathbf{K}$ being a symmetric positive definite matrix for simplicity. Moreover, $\mathbf{u_{s2}}$ is a feedback used to attenuate the effect of model uncertainties for a guaranteed robust performance. Noting Assumption 1 and (P4), there exists a $\mathbf{u_{s2}}$ such that the following two conditions are satisfied [24]:

$$\begin{aligned} &\text{i)} \quad \mathbf{s^T}\left[\mathbf{u_{s2}} - \Psi(\mathbf{q}, \dot{\mathbf{q}}, t)\widetilde{\theta} + \widetilde{\Delta}\right] \le \eta \\ &\text{ii)} \quad \mathbf{s^T u_{s2}} \le \mathbf{0} \end{aligned} \tag{24}$$

where η is a design parameter that can be arbitrarily small. One smooth example of $\mathbf{u_{s2}}$ satisfying (24) is given by $\mathbf{u_{s2}} = -(1/4\eta)h^2\mathbf{s}$, where h is a smooth function satisfying $h \ge \|\theta_{\mathbf{M}}\|\,\|\Psi(\mathbf{q}, \dot{\mathbf{q}}, t)\| + \delta_\Delta$, and $\theta_{\mathbf{M}} = \theta_{\max} - \theta_{\min}$. Using the same derivations as in [29], the following can be shown.

Theorem 1: With the adaptation function in (13) chosen as

$$\boldsymbol{\tau} = \Psi^{\mathbf{T}}(\mathbf{q}, \dot{\mathbf{q}}, t)\mathbf{s} \tag{25}$$

the ARC control law (21) guarantees the following.

1) In general, all signals are bounded with $V(t)$ defined by (17) bounded above by

$$V(t) \le \exp(-\lambda t)V(0) + \frac{\eta}{\lambda}\left[1 - \exp(-\lambda t)\right] \tag{26}$$

where $\lambda = 2\sigma_{\min}(\mathbf{K})/\mu_2$, and $\sigma_{\min}(\cdot)$ denotes the minimum eigenvalue of a matrix.

2) If, after a finite time t_0, there exist parametric uncertainties only, i.e., $\widetilde{\Delta} = 0 \quad \forall t \ge t_0$, then, in addition to result 1), zero steady-state tracking error is also achieved, i.e., $\varepsilon \to 0$ and $\mathbf{s} \to 0$ as $t \to \infty$.

V. DCARC

The DCARC law [27], in which the regressor is calculated by the desired trajectory information only to reduce the effect of measurement noise, has been shown to outperform ARC in terms of all indices [30]. In the following, a DCARC law employing the cogging force model in (5) is constructed and applied to the biaxial linear-motor-driven gantry as well.

The proposed DCARC law and adaptation function have the same form as (21) and (25), but with the regressor $\Psi(\mathbf{q}, \dot{\mathbf{q}}, t)$ substituted by the desired regressor $\Psi_{\mathbf{d}}(\mathbf{q_d}(t), \dot{\mathbf{q}}_{\mathbf{d}}(t), t)$

$$\mathbf{u_t} = \mathbf{u_a} + \mathbf{u_s} \qquad \mathbf{u_a} = -\Psi_{\mathbf{d}}\widehat{\theta} \qquad \boldsymbol{\tau} = \Psi_{\mathbf{d}}^{\mathbf{T}}\mathbf{s}. \tag{27}$$

Choose a p.s.d. function

$$V(t) = \frac{\mathbf{1}}{\mathbf{2}}\mathbf{s^T M_t s} + \frac{\mathbf{1}}{\mathbf{2}}\varepsilon^{\mathbf{T}}\mathbf{K}_\varepsilon\varepsilon \tag{28}$$

where $\mathbf{K}_\varepsilon$ is a diagonal positive definite matrix. Differentiating $V(t)$ and substituting (27) into the resulting expression yield

$$\dot{V} = \mathbf{s^T}[\mathbf{u_s} + \widetilde{\Psi}\theta - \Psi_{\mathbf{d}}\widetilde{\theta} + \widetilde{\Delta}] + \varepsilon^{\mathbf{T}}\mathbf{K}_\varepsilon\dot{\varepsilon} \tag{29}$$

where $\widetilde{\Psi} = \Psi(\mathbf{q}, \dot{\mathbf{q}}, t) - \Psi_{\mathbf{d}}(\mathbf{q_d}, \dot{\mathbf{q}}_{\mathbf{d}}, t)$ is the difference between the actual regression matrix and the desired regression matrix formulations. Similar to those in [31], $\widetilde{\Psi}$ can be quantified as

$$\|\widetilde{\Psi}\theta\| \le \zeta_1\|\varepsilon\| + \zeta_2\|\varepsilon\|^2 + \zeta_3\|\mathbf{s}\| + \zeta_4\|\mathbf{s}\|\|\varepsilon\| \tag{30}$$

where $\zeta_1, \zeta_2, \zeta_3$, and ζ_4 are the positive bounding constants that depend on the desired contour and the physical properties of the biaxial gantry. As in (23), the robust control function $\mathbf{u_s}$ consists of two terms given by

$$\mathbf{u_s} = \mathbf{u_{s1}} + \mathbf{u_{s2}} \qquad \mathbf{u_{s1}} = -\mathbf{K}\mathbf{s} - \mathbf{K}_\varepsilon\varepsilon - \mathbf{K_a}\|\varepsilon\|^2\mathbf{s} \tag{31}$$

where the controller parameters $\mathbf{K}$, $\mathbf{K}_\varepsilon$, and $\mathbf{K_a}$ are diagonal matrices satisfying $\sigma_{\min}(\mathbf{K_a}) \ge \zeta_2 + \zeta_4$ and the following condition:

$$\mathbf{Q} = \begin{bmatrix} \sigma_{\min}(\mathbf{K}_\varepsilon\Lambda) - \frac{1}{4}\zeta_2 & -\frac{1}{2}\zeta_1 \\ -\frac{1}{2}\zeta_1 & \sigma_{\min}(\mathbf{K}) - \zeta_3 - \frac{1}{4}\zeta_4 \end{bmatrix} > 0. \tag{32}$$

For example, by choosing

$$\sigma_{\min}(\mathbf{K}_\varepsilon\Lambda) \ge \frac{1}{2}\zeta_1 + \frac{1}{4}\zeta_2 \qquad \sigma_{\min}(\mathbf{K}) \ge \frac{1}{2}\zeta_1 + \zeta_3 + \frac{1}{4}\zeta_4 \tag{33}$$

it can be verified that the matrix $\mathbf{Q}$ in (32) is positive definite. The same as in (24), the robust control term $\mathbf{u_{s2}}$ is required to satisfy the following conditions:

$$\begin{aligned} &\text{i)} \quad \mathbf{s^T}\{\mathbf{u_{s2}} - \Psi_{\mathbf{d}}\widetilde{\theta} + \widetilde{\Delta}\} \le \eta \\ &\text{ii)} \quad \mathbf{s^T u_{s2}} \le \mathbf{0}. \end{aligned} \tag{34}$$

One smooth example of $\mathbf{u_{s2}}$ satisfying (34) is $\mathbf{u_{s2}} = -(1/4\eta)h_d^2\mathbf{s}$, where h_d is any function satisfying $h_d \ge \|\boldsymbol{\theta}_{\mathbf{M}}\|\,\|\Psi_{\mathbf{d}}\| + \delta_\Delta$. As in [29], the following can be shown.

Theorem 2: The DCARC law (27) guarantees the following.

1) In general, all signals are bounded with $V(t)$ of (28) bounded above by

$$V(t) \le \exp(-\lambda t)V(0) + \frac{\eta}{\lambda}\left[1 - \exp(-\lambda t)\right] \tag{35}$$

where $\lambda = (2\sigma_{\min}(\mathbf{Q})/\max[\mu_2, \sigma_{\max}(\mathbf{K}_\varepsilon)])$, and $\sigma_{\max}(\cdot)$ denotes the maximum eigenvalue of a matrix.

2) Suppose that, after a finite time t_0, there exist parametric uncertainties only, i.e., $\widetilde{\Delta} = 0 \quad \forall\, t \ge t_0$. Then, in addition to result 1), zero steady-state tracking error is achieved as well, i.e., $\varepsilon \to 0$ and $\mathbf{s} \to 0$ as $t \to \infty$.

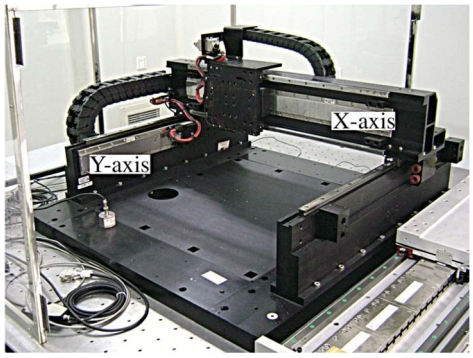

Fig. 2. Biaxial linear-motor-driven gantry system.

VI. Experimental Setup and Results

A. Experiment Setup

A biaxial Anorad HERC-510-510-AA1-B-CC2 gantry from Rockwell Automation is set up in Zhejiang University as a test bed. As shown in Fig. 2, the two axes powered by Anorad LC-50-200 iron core linear motors are mounted orthogonally with X-axis on top of the Y-axis. The position sensors of the gantry are two linear encoders with a resolution of 0.5 μm after quadrature. The velocity signal is obtained by the difference of two consecutive position measurements. Standard least square identification is performed to obtain the parameters of the biaxial gantry, and it is found that the nominal values of the gantry system parameters without loads are $M_1 = 0.12$ V/m/s^2, $M_2 = 0.64$ V/m/s^2, $B_1 = 0.166$ V/m/s, $B_2 = 0.24$ V/m/s, $A_{f1} = 0.1$ V, and $A_{f2} = 0.36$ V.

The explicit measurement of cogging force for both axes has been done by blocking the motor and using an external force sensor to measure the blocking forces at zero input voltages. The measured cogging forces are detailed in [23]. The frequency domain analysis of the measured cogging forces indicates that the fundamental period corresponds to the pitch of the magnets of $P = 50$ mm and that the harmonic terms of cogging forces have significant values at frequencies corresponding to $i = 1, 2, 3$ and $j = 1, 6, 12$ in (5). Thus, the approximate cogging force model (5) is chosen as

$$\begin{aligned}\overline{\mathbf{F}}_{\mathbf{r}}(\mathbf{q}) = \Bigg[& S_{x1}\sin\left(\frac{2\pi}{P}x\right) + C_{x1}\cos\left(\frac{2\pi}{P}x\right) \\ & + S_{x2}\sin\left(\frac{4\pi}{P}x\right) + C_{x2}\cos\left(\frac{4\pi}{P}x\right) \\ & + S_{x3}\sin\left(\frac{6\pi}{P}x\right) + C_{x3}\cos\left(\frac{6\pi}{P}x\right), \\ & \times S_{y1}\sin\left(\frac{2\pi}{P}y\right) + C_{y1}\cos\left(\frac{2\pi}{P}y\right) \\ & + S_{y6}\sin\left(\frac{12\pi}{P}y\right) + C_{y6}\cos\left(\frac{12\pi}{P}y\right) \\ & + S_{y12}\sin\left(\frac{24\pi}{P}y\right) + C_{y12}\cos\left(\frac{24\pi}{P}y\right)\Bigg]^{\mathrm{T}}. \end{aligned} \tag{36}$$

The bounds of the parametric variations are chosen as

$$\begin{aligned}\theta_{\min} = [&0.06, 0.5, 0.15, 0.1, 0.05, 0.08, -0.2, -0.2, \\ &-0.2, -0.2, -0.2, -0.2, -0.2, -0.2, -0.2, \\ &-0.2, -0.2, -0.2, -0.5, -1]^{\mathrm{T}} \\ \theta_{\max} = [&0.20, 0.75, 0.35, 0.3, 0.15, 0.5, 0.2, 0.2, 0.2, 0.2, \\ &0.2, 0.2, 0.2, 0.2, 0.2, 0.2, 0.2, 0.2, 0.5, 1]^{\mathrm{T}}. \end{aligned}$$

B. Performance Indices

As in [30], the following performance indices will be used to measure the quality of each control algorithm.

1) $\|\varepsilon_c\|_{\mathrm{rms}} = ((1/T)\int_0^{\mathrm{T}} |\varepsilon_c|^2\, dt)^{1/2}$, the root-mean-square value of the contouring error, is used to measure the average contouring performance, where T is the total running time.
2) $\varepsilon_{cM} = \max_t\{|\varepsilon_c|\}$, the maximum absolute value of the contouring error, is used to measure transient performance.
3) $\|u_i\|_{\mathrm{rms}} = ((1/T)\int_0^{\mathrm{T}} |u_i|^2\, dt)^{1/2}$, the average control input of each axis, is used to evaluate the amount of control effort.

C. Experimental Results

The control algorithms are implemented using a dSPACE DS1103 controller board. The controller executes programs at a sampling period of $T_s = 0.2$ ms, resulting in a velocity measurement resolution of 0.0025 m/s. The following control algorithms are compared.

1) **C1:** DCARC without cogging force compensation. The smooth functions $S_f(\dot{x}_d)$ and $S_f(\dot{y}_d)$ are chosen as $(2/\pi)\arctan(9000\dot{x}_d)$ and $(2/\pi)\arctan(9000\dot{y}_d)$. The design parameter Λ is chosen as $\Lambda = \mathrm{diag}[100, 30]$. $\mathbf{u_{s2}}$ in (31) is given in Section V. Theoretically, we should use the form of $\mathbf{u_{s2}} = -\mathbf{K_{s2}}(\mathbf{q})\mathbf{s}$ with $\mathbf{K_{s2}}(\mathbf{q})$ being a nonlinear proportional feedback gain as given in [26] to satisfy the robust performance requirement (34) globally. In implementation, a large enough constant feedback gain $\mathbf{K_{s2}}$ is used instead to simplify the resulting control law. With such a simplification, although the robust performance condition (34) may not be guaranteed globally, the condition can still be satisfied in a large enough working range which might be acceptable to practical applications, as done in [32]. With this simplification, noting (31), we choose $\mathbf{u_s} = -\mathbf{K_s}\mathbf{s} - \mathbf{K}_\varepsilon\varepsilon - \mathbf{K_a}\|\varepsilon\|^{\mathbf{2}}\mathbf{s}$ in the experiments, where $\mathbf{K_s}$ represents the combined gain of $\mathbf{K}$ and $\mathbf{K_{s2}}$, and the controller parameters are $\mathbf{K_s} = \mathrm{diag}[100, 60]$, $\mathbf{K_a} = \mathrm{diag}[10\,000, 10\,000]$, and $\mathbf{K}_\varepsilon = \mathrm{diag}[5000, 5000]$. The adaptation rates are set as $\Gamma = \mathrm{diag}[10, 10, 10, 10, 1, 1, 0, 0, 0, 0, 0, 0, 0, 0, 0, 0, 0, 0, 0, 0, 5000, 5000]$. The initial parameter estimates are chosen as $\widehat{\theta}(0) = [0.1, 0.55, 0.20, 0.22, 0.1, 0.15, 0, 0, 0, 0, 0, 0, 0, 0, 0, 0, 0, 0, 0, 0, 0]^{\mathrm{T}}$.

TABLE I
CIRCULAR CONTOURING RESULTS

	Set 1		Set 2		Set 3	
Controller	C1	C2	C1	C2	C1	C2
$\|\|\varepsilon_c\|\|_{rms}(\mu m)$	2.54	1.64	2.66	1.74	3.03	2.11
$\varepsilon_{cM}(\mu m)$	9.22	7.05	9.56	7.91	28.48	25.26
$\|\|u_x\|\|_{rms}(V)$	0.26	0.26	0.26	0.26	0.26	0.26
$\|\|u_y\|\|_{rms}(V)$	0.41	0.41	0.42	0.42	0.41	0.41

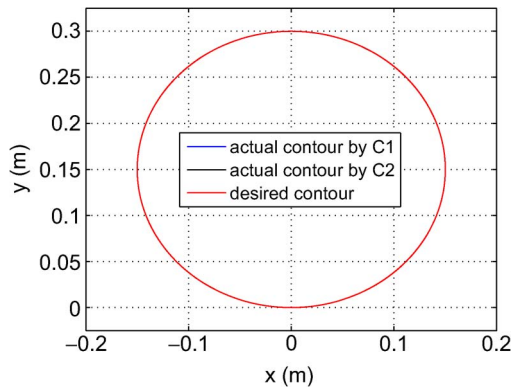

Fig. 3. Circular contouring of Set 1 in the XY plane.

2) **C2:** DCARC with cogging force compensation. The same control law as the aforementioned DCARC but with cogging force compensation, i.e., letting $\Gamma = \text{diag}[10, 10, 10, 10, 1, 1, 500, 500, 500, 500, 500, 500, 500, 500, 500, 500, 500, 500, 5000, 5000]$.

The following test sets are performed.

Set 1) To test the nominal contouring performance of the controllers, experiments are run without payload.

Set 2) To test the performance robustness of the algorithms to parameter variations, a 5-kg payload is mounted on the gantry.

Set 3) A step disturbance (a simulated 0.6-V electrical signal) is added to the input of Y-axis at $t = 1.9$ s and removed at $t = 4.9$ s to test the performance robustness of each controller to disturbance.

1) Circular Contouring With Constant Velocity: To test the contouring performance of the proposed algorithms, the biaxial gantry is first commanded to track a circle given by

$$\mathbf{q_d} = \begin{bmatrix} x_d(t) \\ y_d(t) \end{bmatrix} = \begin{bmatrix} 0.15\sin(2t) \\ -0.15\cos(2t) + 0.15 \end{bmatrix} \tag{37}$$

which has a desired velocity of $\nu = 0.3$ m/s on the contour.

The circular contouring experimental results in terms of performance indices after running the gantry for one period are given in Table I. Overall, both C1 and C2 achieve good steady-state contouring performance during fast circular movements. As shown in the table, C2 performs much better than C1 in terms of all the indices with using almost the same amount of control efforts for every test set. For Set 1, the desired circle and the actual contours by C1 and C2 are shown in Fig. 3, and the contouring errors are shown in Fig. 4, demonstrating the good nominal performance of DCARC controllers—the contour errors are mostly within 5 μm. For Set 2, the contouring errors are shown in Fig. 5 which shows that both controllers achieve good steady-state contouring performance in spite of the change of inertia load, verifying the performance robustness of the proposed DCARC controllers to parameter variations. The contouring errors of Set 3 are shown in Fig. 6. As shown in the figures, the added large disturbances do not affect the contouring performance much except the transient spikes when the sudden changes of the disturbances occur—even the transient tracking errors are within 26 μm for C2. These results demonstrate the strong performance robustness of the DCARC schemes. Comparing C2 with C1, the improvements of contouring performances in all three sets also illustrate the effectiveness of the cogging force compensations.

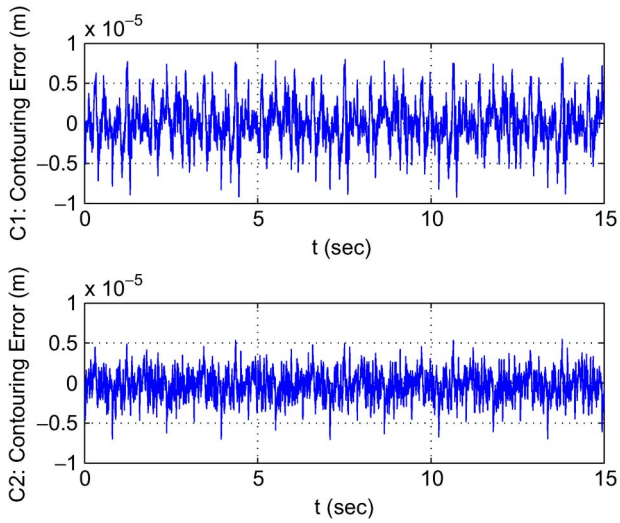

Fig. 4. Circular contouring errors of Set 1 (no load).

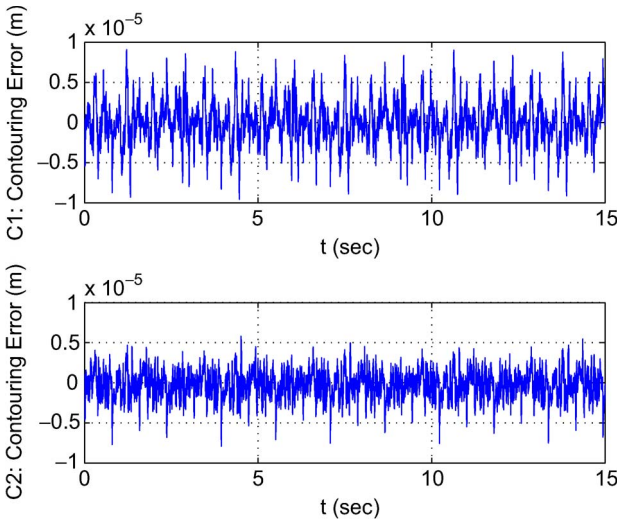

Fig. 5. Circular contouring errors of Set 2 (loaded).

2) Elliptical Contouring: To test the contouring performance of the proposed algorithms for noncircular motions, the biaxial gantry is also commanded to track an ellipse described by

$$\mathbf{q_d} = \begin{bmatrix} x_d(t) \\ y_d(t) \end{bmatrix} = \begin{bmatrix} 0.2\sin(3t) \\ -0.1\cos(3t) + 0.1 \end{bmatrix} \tag{38}$$

which has a constant angular velocity of $\omega = 3$ rad/s but a time-varying feed rate.

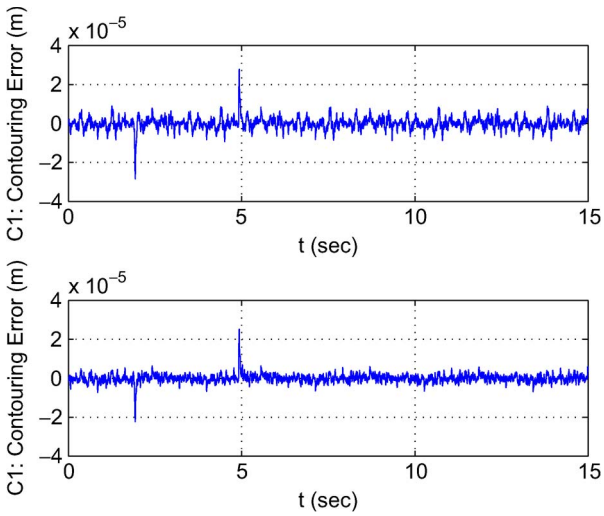

Fig. 6. Circular contouring errors of Set 3 (disturbances).

TABLE II
ELLIPTICAL CONTOURING RESULTS

	Set 1		Set 2		Set 3	
Controller	C1	C2	C1	C2	C1	C2
$\|\|\varepsilon_c\|\|_{rms}(\mu m)$	2.66	2.06	2.74	2.10	3.43	2.93
$\varepsilon_{cM}(\mu m)$	8.77	7.33	9.69	8.55	31.03	29.46
$\|\|u_x\|\|_{rms}(V)$	0.35	0.35	0.37	0.37	0.35	0.35
$\|\|u_y\|\|_{rms}(V)$	0.50	0.50	0.52	0.51	0.50	0.50

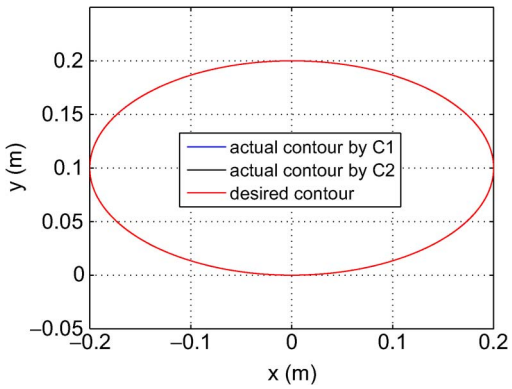

Fig. 7. Elliptical contouring of Set 1 in the XY plane.

The elliptical contouring experimental results in terms of performance indices after running the gantry for one period are given in Table II. Overall, both C1 and C2 achieve good steady-state contouring performance during the fast elliptical movements. As can be seen from the table, C2 performs better than C1 in terms of all the indices with using almost the same amount of control efforts for every test set. For Set 1, the desired ellipse and the actual contours by C1 and C2 are shown in Fig. 7, and the contouring errors are shown in Fig. 8, which are mostly within 5 μm as well. For Set 2, the contouring errors are shown in Fig. 9, which are almost the same as those without the payload, demonstrating the strong performance robustness of both controllers to the change of inertia load. The contouring errors of Set 3 are given in Fig. 10. Again, the added large disturbances do not affect the contouring performance much except the initial transient when the sudden changes of the

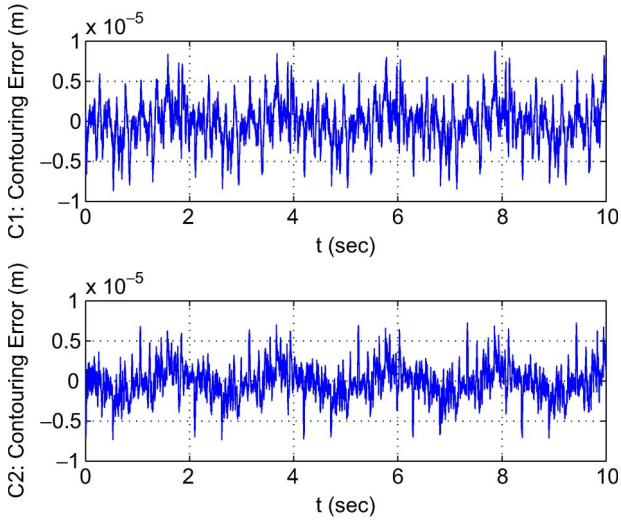

Fig. 8. Elliptical contouring errors of Set 1 (no load).

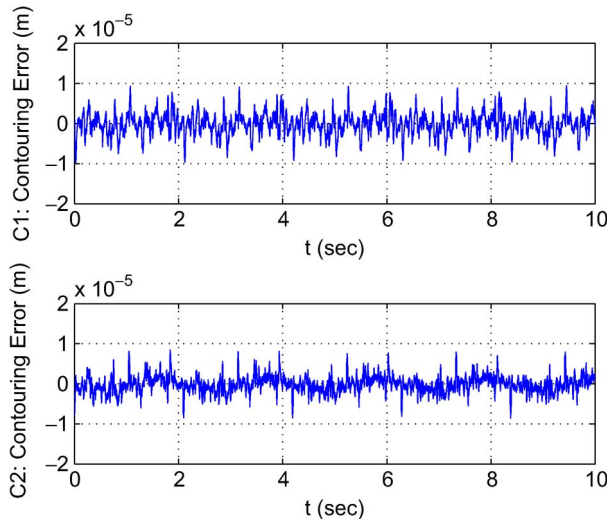

Fig. 9. Elliptical contouring errors of Set2 (loaded).

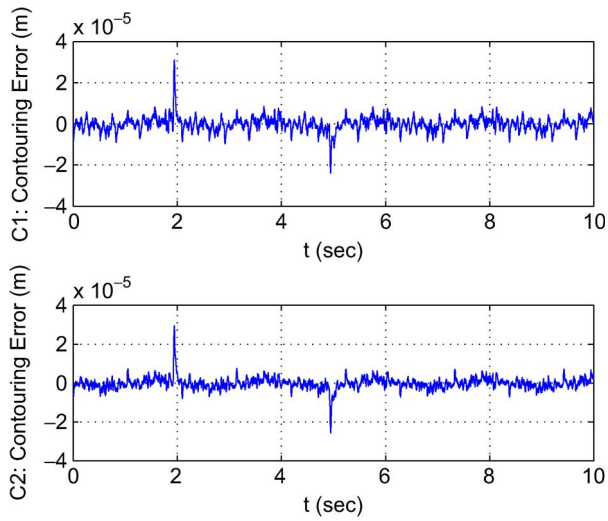

Fig. 10. Elliptical contouring errors of Set 3 (disturbances).

disturbances occur. All these results further demonstrate the strong performance robustness of the proposed schemes and the effectiveness of the cogging force compensations.

VII. Conclusion

This paper has studied the high-performance contouring motion control of an industrial biaxial linear-motor-driven precision gantry subject to significant nonlinear cogging force effects. A DCARC controller has been developed under the task coordinate formulation. The proposed controller explicitly takes into account the effect of model uncertainties coming from the inertia load, friction forces, cogging forces, and external disturbances. In particular, based on the special structure of the cogging forces, design models consisting of known basis functions with unknown weights are used to approximate the unknown nonlinear cogging forces in both axes. The resulting controller guarantees a prescribed contouring performance in general while achieving asymptotic tracking in the presence of parametric uncertainties only. Experimental results for both high-speed circular and elliptical motions have demonstrated the excellent contouring performance of the proposed DCARC scheme in actual applications and the strong performance robustness to parameter variations and disturbances. Comparative experimental results have also been presented to verify the effectiveness of the proposed cogging force compensations.

References

[1] M.-Y. Cheng and C.-C. Lee, "Motion controller design for contour-following tasks based on real-time contour error estimation," *IEEE Trans. Ind. Electron.*, vol. 54, no. 3, pp. 1686–1695, Jun. 2007.

[2] P. Y. Li, "Coordinated contour following control for machining operations—A survey," in *Proc. Amer. Control Conf.*, 1999, pp. 4543–4547.

[3] G. T. C. Chiu and M. Tomizuka, "Contouring control of machine tool feed drive systems: A task coordinate frame approach," *IEEE Trans. Control Syst. Technol.*, vol. 9, no. 1, pp. 130–139, Jan. 2001.

[4] M. Jin, S. H. Kang, and P. H. Chang, "Robust compliant motion control of robot with nonlinear friction using time-delay estimation," *IEEE Trans. Ind. Electron.*, vol. 55, no. 1, pp. 258–269, Jan. 2008.

[5] R. Martinez, J. Alvarez, and Y. Orlov, "Hybrid sliding-mode-based control of underactuated systems with dry friction," *IEEE Trans. Ind. Electron.*, vol. 55, no. 11, pp. 3998–4003, Nov. 2008.

[6] R. Cao and K. Low, "A repetitive model predictive control approach for precision tracking of a linear motion system," *IEEE Trans. Ind. Electron.*, vol. 56, no. 6, pp. 1955–1962, Jun. 2009.

[7] T.-S. Hwang and J.-K. Seok, "Observer-based ripple force compensation for linear hybrid stepping motor drives," *IEEE Trans. Ind. Electron.*, vol. 54, no. 5, pp. 2417–2424, Oct. 2007.

[8] K. Gulez, A. A. Adam, and H. Pastaci, "Torque ripple and EMI noise minimization in PMSM using active filter topology and field-oriented control," *IEEE Trans. Ind. Electron.*, vol. 55, no. 1, pp. 251–257, Jan. 2008.

[9] F.-J. Lin and P.-H. Chou, "Adaptive control of two-axis motion control system using interval type-2 fuzzy neural network," *IEEE Trans. Ind. Electron.*, vol. 56, no. 1, pp. 178–193, Jan. 2009.

[10] Y.-S. Kung, R.-F. Fung, and T.-Y. Tai, "Realization of a motion control IC for x–y table based on novel FPGA technology," *IEEE Trans. Ind. Electron.*, vol. 56, no. 1, pp. 43–53, Jan. 2009.

[11] Y. Koren and C. C. Lo, "Variable gain cross coupling controller for contouring," *Ann. CIRP*, vol. 40, no. 1, pp. 371–374, 1991.

[12] S.-S. Yeh and P.-L. Hsu, "Estimation of the contouring error vector for the cross-coupled control design," *IEEE/ASME Trans. Mechatronics*, vol. 7, no. 1, pp. 44–51, Mar. 2002.

[13] Y. Xiao and K. Y. Zhu, "Optimal synchronization control of high-precision motion systems," *IEEE Trans. Ind. Electron.*, vol. 53, no. 4, pp. 1160–1169, Jun. 2006.

[14] K.-H. Su and M.-Y. Cheng, "Contouring accuracy improvement using cross-coupled control and position error compensator," *Int. J. Mach. Tools Manuf.*, vol. 48, no. 12/13, pp. 1444–1453, Oct. 2008.

[15] Y. Koren, "Cross-coupled biaxial computer control for manufacturing systems," *Trans. ASME, J. Dyn. Syst., Meas., Control*, vol. 102, no. 4, pp. 265–272, Dec. 1980.

[16] B. Yao, S. P. Chan, and D. Wang, "Unified formulation of variable structure control schemes to robot manipulators," *IEEE Trans. Autom. Control*, vol. 39, no. 2, pp. 371–376, Feb. 1994.

[17] T. C. Chiu and B. Yao, "Adaptive robust contour tracking of machine tool feed drive systems—A task coordinate frame approach," in *Proc. Amer. Control Conf.*, 1997, vol. 5, pp. 2731–2735.

[18] L. Xu and B. Yao, "Coordinated adaptive robust contour tracking of linear-motor-driven tables in task space," in *Proc. IEEE Conf. Decision Control*, Sydney, Australia, 2000, pp. 2430–2435.

[19] C.-L. Chen and K.-C. Lin, "Observer-based contouring controller design of a biaxial stage system subject to friction," *IEEE Trans. Control Syst. Technol.*, vol. 16, no. 2, pp. 322–329, Mar. 2008.

[20] L. Xu and B. Yao, "Adaptive robust precision motion control of linear motors with ripple force compensation: Theory and experiments," in *Proc. IEEE Conf. Control Appl.*, Anchorage, AK, 2000, pp. 373–378.

[21] S. Zhao and K. Tan, "Adaptive feedforward compensation of force ripples in linear motors," *Control Eng. Pract.*, vol. 13, no. 9, pp. 1081–1092, Sep. 2005.

[22] B. Yao, C. Hu, and Q. Wang, "Adaptive robust precision motion control of high-speed linear motors with on-line cogging force compensations," in *Proc. IEEE/ASME Conf. Adv. Intell. Mechatronics*, Zurich, Switzerland, 2007, pp. 1–6.

[23] L. Lu, Z. Chen, B. Yao, and Q. Wang, "Desired compensation adaptive robust control of a linear motor driven precision industrial gantry with improved cogging force compensation," *IEEE/ASME Trans. Mechatronics*, vol. 13, no. 6, pp. 617–624, Dec. 2008.

[24] B. Yao, "High performance adaptive robust control of nonlinear systems: A general framework and new schemes," in *Proc. IEEE Conf. Decision Control*, San Diego, CA, 1997, pp. 2489–2494.

[25] B. Yao and M. Tomizuka, "Smooth robust adaptive sliding mode control of robot manipulators with guaranteed transient performance," *Trans. ASME, J. Dyn. Syst., Meas., Control*, vol. 118, no. 4, pp. 764–775, Dec. 1996.

[26] B. Yao and M. Tomizuka, "Adaptive robust control of SISO nonlinear systems in a semi-strict feedback form," *Automatica*, vol. 33, no. 5, pp. 893–900, May 1997.

[27] B. Yao, "Desired compensation adaptive robust control," *Trans. ASME, J. Dyn. Syst., Meas., Control*, vol. 131, no. 6, pp. 061001-1–061001-7, Nov. 2009.

[28] B. Yao and L. Xu, "Adaptive robust control of linear motors for precision manufacturing," *Mechatronics*, vol. 12, no. 4, pp. 595–616, May 2002.

[29] C. Hu, B. Yao, and Q. Wang, "Coordinated adaptive robust contouring controller design for an industrial biaxial precision gantry," *IEEE/ASME Trans. Mechatronics*, to be published.

[30] L. Xu and B. Yao, "Adaptive robust precision motion control of linear motors with negligible electrical dynamics: Theory and experiments," *IEEE/ASME Trans. Mechatronics*, vol. 6, no. 4, pp. 444–452, Dec. 2001.

[31] N. Sadegh and R. Horowitz, "Stability and robustness analysis of a class of adaptive controllers for robot manipulators," *Int. J. Robot. Res.*, vol. 9, no. 3, pp. 74–92, Jun. 1990.

[32] B. Yao, F. Bu, J. Reedy, and G. Chiu, "Adaptive robust control of single-rod hydraulic actuators: Theory and experiments," *IEEE/ASME Trans. Mechatronics*, vol. 5, no. 1, pp. 79–91, Mar. 2000.

Chuxiong Hu (S'09) received the B.Eng. degree from Zhejiang University, Hangzhou, China, in 2005, where he is currently working toward the Ph.D. degree in mechatronic control engineering.

His research interests include coordinated motion control, precision mechatronics, adaptive control, robust control, and nonlinear systems.

Bin Yao (S'92–M'96–SM'09) received the B.Eng. degree in applied mechanics from Beijing University of Aeronautics and Astronautics, Beijing, China, in 1987, the M.Eng. degree in electrical engineering from Nanyang Technological University, Singapore, in 1992, and the Ph.D. degree in mechanical engineering from the University of California, Berkeley, in 1996.

Since 1996, he has been with the School of Mechanical Engineering, Purdue University, West Lafayette, IN, where he became a Professor in 2007. He was honored as a Kuang-Piu Professor at Zhejiang University, Hangzhou, China, in 2005. He has been an Associate Editor of the *ASME Journal of Dynamic Systems, Measurement, and Control* since 2006.

Dr. Yao was the recipient of the Faculty Early Career Development Award from the National Science Foundation in 1998, the Joint Research Fund for Outstanding Overseas Chinese Young Scholars from the National Natural Science Foundation of China in 2005, the O. Hugo Schuck Best Paper (Theory) Award from the American Automatic Control Council in 2004, and the Outstanding Young Investigator Award of the ASME Dynamic Systems and Control Division (DSCD) in 2007. He has chaired numerous sessions and served on the International Program Committees of various IEEE, ASME, and International Federation of Automatic Control conferences. He was the Chair of the Adaptive and Optimal Control Panel from 2000 to 2002 and the Fluid Control Panel of the ASME DSCD from 2001 to 2003. He is currently the Vice-Chair of the ASME DSCD Mechatronics Technical Committee. He was a Technical Editor of the IEEE/ASME TRANSACTIONS ON MECHATRONICS from 2001 to 2005.

Qingfeng Wang received the M.Eng. and Ph.D. degrees in mechanical engineering from Zhejiang University, Hangzhou, China, in 1988 and 1994, respectively.

Since 1994, he has been with Zhejiang University, where he became a Professor in 1999, was the Director of the State Key Laboratory of Fluid Power Transmission and Control from 2001 to 2005, and currently serves as the Director of the Institute of Mechatronic Control Engineering. His research interests include electrohydraulic control components and systems, hybrid power system and energy saving techniques for construction machinery, and system synthesis for mechatronic equipment.